3D Displacement Field Reconstruction from Planar Tagged Cardiac MR Images

Thomas S. Denney Jr. Jerry L. Prince

Department of Electrical and Computer Engineering
Johns Hopkins University
Baltimore, MD 21218

Abstract

A major problem in cardiac imaging is the measurement of cardiac motion for identification of ischemic and infarcted tissues. O'Dell et. al. have recently proposed a method that uses magnetic resonance tag patterns to measure the 3D displacement field of the myocardium. The measurements are sparse, however, and interpolation is required to reconstruct a dense displacement field. In this paper, we propose a method for computing a dense displacement field on a regular 3D lattice from sparse displacement measurements. This method uses a multidimensional stochastic model for the true displacement field and the Fisher estimation framework to estimate a displacement vector at each point the lattice. Simulation results are presented that demonstrate the accuracy of our technique.

1 Introduction

A major problem in cardiac imaging is the measurement of cardiac motion for identification of ischemic and infarcted tissues. Magnetic resonance tagging has shown great potential for noninvasive measurement of the motion of the beating heart. Tagged images appear with a spatially encoded pattern that moves with the tissue and can be analyzed to reveal the motion of the myocardium from which measures of local contractile performance such as strain can be extracted.

The use of planar tags has been studied by several researchers [1, 2, 3, 4, 5, 6, 7, 8, 9]. In the approach of Zerhouni et al [1, 2], thin sheet tags are placed to pass through the long axis of the LV at different angular orientations. Images taken orthogonal to this axis appear to have a tag "starburst" pattern emanating from the cardiac chamber. After identifying inner and outer contours and the tag "spines" through image analysis techniques [5], the motion can be characterized by matching points of intersection of tags with contours. Another technique for embedding tags within the myocardium is based on the method of spatial modulation of magnetization (SPAMM) [3, 4, 7], which produces a grid-like array of tag stripes. These methods are efficient since many tags can be placed within the tissue in a very short time. Several methods have been proposed to track the tag grid intersections over the cardiac cycle and compute quantities such as strain [10, 11].

O'Dell et. al. [12] have proposed a method for using parallel planar tags to image the 3D displacement field of the myocardium. In their method, a set of tag planes orthogonal to the x-axis are applied to the heart at end-diastole. A stack of 2D short-axis images is acquired at both end-diastole and end-systole. The tag lines, which appear straight in the reference image, appear curved in the deformed image (as depicted in Figures 3 and 4). The positions of points along these curved lines are then determined using a semi-automated tracking method (see [13]). The displacement of the heart in the x-direction can be measured by comparing the locations of the reference and deformed tag lines. The y-displacement can be measured by applying a set of tag planes in the orthogonal direction and acquiring another set of short-axis images. Applying tag planes orthogonal to the z-axis and acquiring a set of long-axis images is used to measure the z-displacement.

In effect, this method measures the 3D displacement field of the heart one component at a time. The displacement measurements, however, are sparse; interpolation is required to reconstruct a dense displacement field from which strain can be computed. O'Dell et. al [12] proposed fitting a high order polynomial to the displacement measurements. The choice of a polynomial basis function is arbitrary, however, and

0-8186-5802-9/94 $3.00

the correct order of the interpolating polynomial is not known. Young and Axel [11] proposed fitting displacement measurements from grid-tagged images to a finite-element model of the heart.

In this paper, we propose a method for reconstructing the heart's displacement field on a regular 3D lattice from sparse displacement measurements. This method uses a multidimensional stochastic model for the displacement field and the Fisher estimation framework [14] to estimate a displacement vector at each point on the lattice. Simulation results are presented that show an estimation accuracy comparable to other proposed methods. Our method has two main advantages. First, the displacement field model makes a fairly weak assumption on the specifics of heart motion. Second, the Fisher estimate provides an a priori error covariance that can be used to determine the minimum number of tag lines needed to achieve a given estimation accuracy.

This paper is organized as follows. In Section 2 we present some background on the geometry of planar tagged images and establish some notation. In Section 3 we derive our reconstruction method. In Section 4 we present simulation results to demonstrate the accuracy of our method. In Section 5, we provide a discussion of our results and some directions for future work.

2 Background

2.1 Notation

In this paper, scalars are designated by lower-case letters (e.g. x, a), and 3D vectors are designated by lower-case bold letters (e.g. $\mathbf{u}$, $\mathbf{r}$). Lexicographically ordered vector fields and matrices are designated by upper-case letters (e.g. U, V).

Two coordinate systems are used to describe the location of points in space. A material coordinate system is fixed on the left ventricle (LV), where end-diastole is used as the reference state. A spatial coordinate system is fixed in space, where the material and spatial coordinate systems coincide at end-diastole. The z-axis of the spatial coordinate system corresponds to the slice select direction of the MR imaging protocol for a short-axis slice of the LV. Typically, this axis runs through the center of the LV at end-diastole from apex to base. The x and y axes are orthogonal to the z-axis and to each other. The x-axis is parallel to the top and bottom edges of a short-axis image.

2.2 Geometry of planar tagged images

In the 3D displacement field measurement technique developed by O'Dell, et. al [12], the data is composed of three sets of 2D images. The first two sets are short-axis images taken at the planes depicted in Figure 1. The third set consists of long-axis images taken at the planes depicted in Figure 2. In each

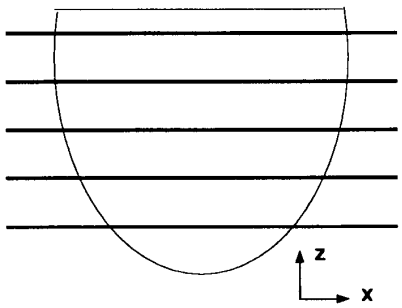

Figure 1: Short-axis image planes.

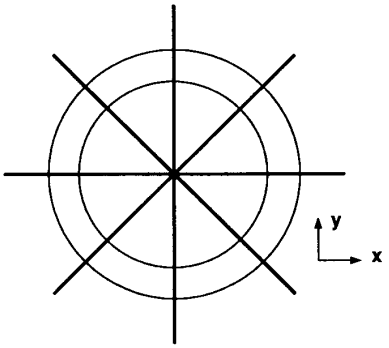

Figure 2: Long-axis image planes.

image set, one component of the displacement field is measured by comparing the positions of deformed and undeformed tag planes. To measure the x-component of the displacement field, a set of parallel tag planes orthogonal to the x-axis are applied to the heart at end-diastole, and a stack of short-axis images is acquired immediately after tagging and at a later point in the cardiac cycle. To measure the y-component, tag planes orthogonal to the y-axis are applied and another set of short-axis images are acquired. To measure the z-component, tag planes orthogonal to the z-axis are applied, and a set of long-axis images are acquired. We refer to tag planes orthogonal to the

x-axis as vertical tags, tag planes orthogonal to the y-axis as horizontal tags and tag plane orthogonal to the z-axis as long-axis tags.

A diagram of the LV in the reference state (end-diastole) with vertical tags is shown in Figure 3. The solid lines show the intersections of the tag planes with the image plane. Figure 4 depicts the LV in a deformed state (e.g. end-systole). The solid lines are the deformed tag lines, and the dashed lines are the original tag lines. The dots on the deformed tag lines rep-

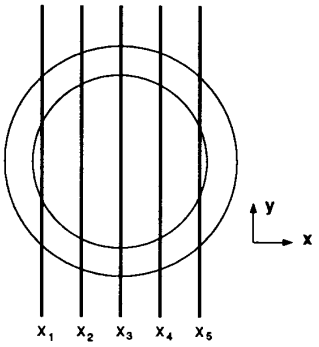

Figure 3: LV at end-diastole (reference) with vertical tags.

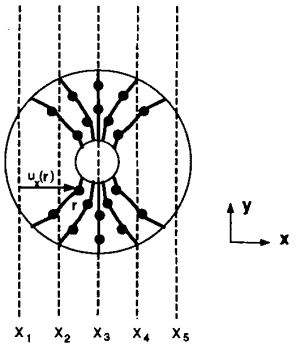

Figure 4: LV at end-systole (deformed).

resent points identified by a tag tracking routine such as the one proposed by Guttman, et. al [13]. Since there is a one-to-one correspondence between the undeformed and deformed tag planes, a point identified on the deformed tag line, $\mathbf{r}$ for example, must have originated at a point on the undeformed tag plane. All points on the jth undeformed tag plane have the same x-coordinate, x_j, and the x-coordinate of $\mathbf{r}$ is known from the tag tracking routine. Therefore the x-displacement of the point $\mathbf{r}$ on tag plane j is given by:

$$u_x(\mathbf{r}) = r_x - x_j \,. \tag{1}$$

The y and z components of the displacement vector $\mathbf{u}(\mathbf{r}) = [u_x(\mathbf{r}),\, u_y(\mathbf{r}),\, u_z(\mathbf{r})]^T$ are unknown.

Thus, the fundamental information from a tagging experiment comprises measurements of the displacement field components. These displacement measurements are sparse, however, and interpolation is required to reconstruct a dense displacement field from which strain can be computed. This reconstruction problem is addressed in Section 3. In addition, since the points are specified in a spatial coordinate system, the displacement vector measurements are defined in spatial coordinates, and the reconstructed displacement field will be a function of spatial coordinates. The displacement field must be transformed into material coordinates before strain can be computed. This transformation problem is addressed in Section 3.4.

3 Reconstruction method

3.1 Measurement model

Our goal is to compute a dense estimate of the left ventricle's displacement field from the sparse measurements provided by the deformed tag lines. A continuous estimate of the displacement field is not feasible because of the complex motion of the LV. As a result, we compute an estimate of the displacement field at each point in a $N_x \times N_y \times N_z$ grid Ω like the one shown in Figure 5. The grid is defined so that it contains the

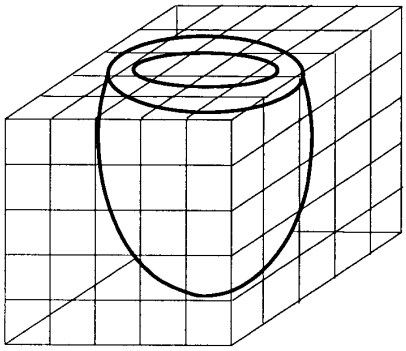

Figure 5: $N_x \times N_y \times N_z$ grid Ω.

entire LV. The grid spacing h can be arbitrarily small, but should be on the order of the MR image pixel size.

As stated in Section 2.2., discrete points on the deformed tag lines are identified by a tag tracking algorithm. Since these points will not in general be on a

grid point, we round the position of each tracked point to the nearest grid point. This rounding will introduce some additional error into the measurement model, which we account for in the measurement noise variance described below. The extent of the error, however, will decrease with smaller grid spacings. More accurate ways of interpolating displacement measurements onto grid points are a subject of future research.

Let Ω_x denote the set of grid points where a x-displacement measurement is defined, and Ω_y and Ω_z be the sets of grid points where y and z-displacement measurements are defined. Note that

$$\Omega_x, \Omega_y, \Omega_z \subset \Omega\,,$$

and Ω_x, Ω_y and Ω_z will, in general, have points in common. We designate the cardinality of Ω_x, Ω_y and Ω_z by M_x, M_y and M_z respectively and let $M = M_x + M_y + M_z$.

The displacement field measurements are described mathematically by the equation

$$y_m(\mathbf{r}) = \mathbf{e}(\mathbf{r}) \cdot \mathbf{u}(\mathbf{r}) + v_m(\mathbf{r})\,, \tag{2}$$

where

$$\mathbf{e}(\mathbf{r}) = \begin{cases} \mathbf{e}_x & \mathbf{r} \in \Omega_x \\ \mathbf{e}_y & \mathbf{r} \in \Omega_y \\ \mathbf{e}_z & \mathbf{r} \in \Omega_z \end{cases}\,, \tag{3}$$

$\mathbf{e}_x$, $\mathbf{e}_y$ and $\mathbf{e}_z$ are the unit vectors corresponding the the x, y and z axes, and $v_m(\mathbf{r}) \sim N(0, \sigma_m^2(\mathbf{r}))$. The measurement noise, v_m, arises from two independent sources. The first source is the error in tracking the tag line. The second is the error incurred from rounding the measured displacement vector to the nearest grid point.

In order to use the estimation technique described below, we stack $\mathbf{u}(\mathbf{r})$ in lexicographical order and stack $y_m(\mathbf{r})$ and $v_m(\mathbf{r})$ into the $M \times 1$ vectors Y_m and V_m. The measurement equation becomes

$$Y_m = EU + V_m\,, \tag{4}$$

where

$$U = \begin{bmatrix} \mathbf{u}(\mathbf{r}_{111}) \\ \mathbf{u}(\mathbf{r}_{112}) \\ \vdots \\ \mathbf{u}(\mathbf{r}_{11N_z}) \\ \mathbf{u}(\mathbf{r}_{121}) \\ \vdots \\ \mathbf{u}(\mathbf{r}_{N_xN_yN_z}) \end{bmatrix}_{N_xN_yN_z \times 1}\,, \tag{5}$$

and $\mathbf{r}_{ijk}$ are the lattice points in Ω. The $M \times N_xN_yN_z$ matrix E is structured such that (2) is satisfied for each measurement.

3.2 Displacement field model

Ideally, one would want to reconstruct the stacked displacement field vector U from equation (4) alone. Since the matrix E is not invertible, however, there are an infinite number of displacement fields that satisfy the measurement equation (4). One could use the Moore-Penrose inverse of E in which case the reconstructed displacement field $\hat{U}$ is given by

$$\hat{U} = E^T(EE^T)^{-1}Y_m\,. \tag{6}$$

Unfortunately, this approach makes the implicit assumption that of all the displacement fields that satisfy (4), we want the one with smallest norm ($\sqrt{U^TU}$) — an assumption that is rather arbitrary from a physiological standpoint.

Our approach is to assume an explicit stochastic model for the displacement field. This model will provide enough additional information to reconstruct the displacement field from the measurements in equation (4). In particular, we model each component of the displacement field as a Brownian surface in analogy to the model proposed in [15, 16, 17] for optical flow estimation of motion. An example of a 2D vector field generated by this type of model is shown in Figure 6 with a mesh plot of each Brownian surface component shown in Figures 7a and 7a. In displacement fields

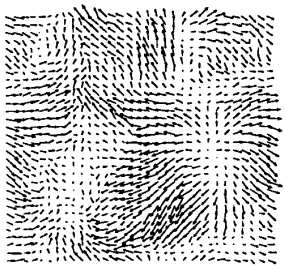

Figure 6: Realization of a random 2D displacement field.

generated by this model, vectors that are close in space have similar magnitude and direction.

A physiological motivation of this model comes from the connected nature of biological tissue, so we expect this model to hold fairly well inside the myocardium. The blood pool inside the LV and the pericardial sac around the heart, however, cause discontinuities in the true displacement field that are not

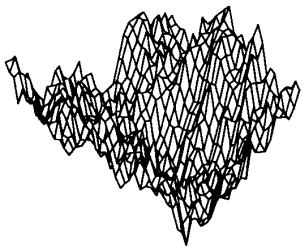

(a)

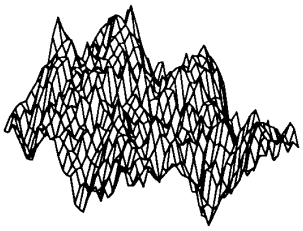

(b)

Figure 7: (a) Mesh plot of x-component. (b) Mesh plot of y-component.

accurately modeled by this model. As a result, we expect the reconstructed displacement field to be more accurate inside the myocardium than at the epicardial and endocardial boundaries.

The smoothness of the displacement field is described by Figure 8. From the definition of displacement, the spatial point $\mathbf{r}$ moves to $\mathbf{r}+\mathbf{u}(\mathbf{r})$ and the spatial point $\mathbf{r}+\mathbf{n}$ moves to $\mathbf{r}+\mathbf{n}+\mathbf{u}(\mathbf{r}+\mathbf{n})$. Our model specifies that for $\mathbf{n}$ small, $\mathbf{u}(\mathbf{r})$ and $\mathbf{u}(\mathbf{r}+\mathbf{n})$ are similar vectors. Specifically, we let $\mathbf{n} \in \{h\mathbf{e}_x, h\mathbf{e}_y, h\mathbf{e}_z\}$ and require that

$$\begin{aligned} \mathbf{u}(\mathbf{r}+h\mathbf{e}_x)-\mathbf{u}(\mathbf{r}) &= \mathbf{v}_x(\mathbf{r}),\ \forall \mathbf{r}, \mathbf{r}+h\mathbf{e}_x \in \Omega \\ \mathbf{u}(\mathbf{r}+h\mathbf{e}_y)-\mathbf{u}(\mathbf{r}) &= \mathbf{v}_y(\mathbf{r}),\ \forall \mathbf{r}, \mathbf{r}+h\mathbf{e}_y \in \Omega \\ \mathbf{u}(\mathbf{r}+h\mathbf{e}_z)-\mathbf{u}(\mathbf{r}) &= \mathbf{v}_z(\mathbf{r})\ \forall \mathbf{r}, \mathbf{r}+h\mathbf{e}_z \in \Omega\,, \end{aligned} \quad (7)$$

where $\forall \mathbf{r} \in \Omega$, $\mathbf{v}_x(\mathbf{r})$, $\mathbf{v}_y(\mathbf{r})$ and $\mathbf{v}_z(\mathbf{r})$ are white random vector processes that have a joint Gaussian density given by $N(0, h^2\sigma_s^2(\mathbf{r})I)$. According to this model, the point $\mathbf{r}+\mathbf{n}$ to moves to a point in a cloud centered

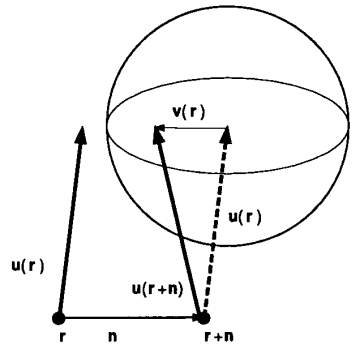

Figure 8: Displacement field smoothness model.

at $\mathbf{r}+\mathbf{n}+\mathbf{u}(\mathbf{r})$ as shown in Figure 8. Note that this formulation only models the value of the displacement vectors relative to each other. Inspection of Equation (7) shows that an arbitrary constant can be added to each component of the displacement field and Equation (7) would still hold. Consequently, the actual value of any particular displacement vector is neither known nor described in a probabilistic sense.

As with the measurement model in equation (4), we stack the equations in (7) in lexicographical order to form the matrix equation

$$SU = V_{xyz}\,, \quad (8)$$

where S is a spatial difference operator and $V_{xyz} = [V_x^T, V_y^T, V_z^T]^T$. The vectors V_x, V_y, V_z contain the lexicographically ordered vector fields $\mathbf{v}_x(\mathbf{r})$, $\mathbf{v}_y(\mathbf{r})$ and $\mathbf{v}_z(\mathbf{r})$ respectively. The structure of S is given by

$$S = \begin{bmatrix} S_x \\ S_y \\ S_z \end{bmatrix}\,, \quad (9)$$

where

$$S_x = \begin{bmatrix} I & -I & & \\ & I & -I & \\ & & \ddots & \\ & & & I \quad -I \end{bmatrix}\,, \quad I = I_{N_x N_y}$$

$S_y = I_{N_z} \otimes \Delta_y$, where

$$\Delta_y = \begin{bmatrix} I & -I & & \\ & I & -I & \\ & & \ddots & \\ & & & I \quad -I \end{bmatrix}\,, \text{and } I = I_{N_x};$$

$S_z = I_{N_x N_y} \otimes \Delta_z$, where

$$\Delta_z = \begin{bmatrix} I & -I & & & \\ & I & -I & & \\ & & \ddots & & \\ & & & I & -I \end{bmatrix}, \text{and } I = I_3,$$

and $\otimes$ is Kronecker product.

This stochastic displacement field model provides the additional equations needed to reconstruct a unique displacement field from the measurements in equation (4). The Brownian surface model is a general model for smooth displacement fields and is *not* intended to specifically model the motion of the heart. While this type of model may not be as accurate for heart motion, it is less dependent on the restrictive and possibly invalid a priori assumptions needed for a more specific model. More sophisticated displacement field models are under development.

3.3 Fisher estimate

Equation (8) is a stochastic model for the displacement field U, and we would like to compute its mean and variance. Unfortunately, the matrix S is singular because $SA = 0$ when A is a nonzero constant vector. As a result we cannot compute the mean and variance of U from (8). Bayesian estimators cannot be used in this case because they require that the mean and variance be known a priori. The Fisher estimation method [14], however, does not require knowledge of the mean and covariance of U; hence, we use this method to reconstruct the displacement field.

While the displacement field model in (8) does not completely specify the statistics of U, we do want to incorporate the information given by the model into the Fisher estimate. The model is not a measurement in the classical sense because it does not change from realization to realization. The model does, however, constrain the solution in the same way that a measurement does.

To capture this concept, we treat the displacement field model in equation (8) as an *a priori observation* on the unknown displacement field U [14]:

$$0 = SU - V_{xyz}\,, \tag{10}$$

and form the augmented system

$$Y = CU + V\,, \tag{11}$$

where

$$Y = \begin{bmatrix} Y_m \\ 0 \end{bmatrix},\ C = \begin{bmatrix} E \\ S \end{bmatrix},\ \text{and } V = \begin{bmatrix} V_m \\ -V_{xyz} \end{bmatrix}. \tag{12}$$

Assuming constant noise variances σ_s^2 and σ_w^2, the optimal estimate $\hat{U}$ is given by

$$\Sigma\hat{U} = \frac{1}{\sigma_w^2} E^T Y_m\,, \tag{13}$$

where

$$\Sigma = \frac{1}{h^2\sigma_s^2}[S_x^T S_x + S_y^T S_y + S_z^T S_z] + \frac{1}{\sigma_w^2} E^T E\,. \tag{14}$$

The difference operators $S_x^T S_x$, $S_y^T S_y$ and $S_z^T S_z$ are the discrete analogs the the continuous operators $\partial^2/\partial x^2$, $\partial^2/\partial y^2$ and $\partial^2/\partial z^2$ respectively. In fact, (13) is exactly the same equation obtained when the partial differential equation

$$-\frac{1}{\sigma_s^2}\nabla^2\mathbf{u} + \frac{1}{\sigma_w^2}\mathbf{e}\mathbf{e}^T\mathbf{u} = \frac{1}{\sigma_w^2}\mathbf{e}y \tag{15}$$

is discretized on the lattice Ω. Equation (13) can be solved using any of the methods commonly used to solve (15) such as SOR [18].

The Fisher estimate minimizes the expected mean-square estimation error subject to the constraint that $\mathcal{E}\{\hat{U}\} = \mathcal{E}\{U\}$ where $\mathcal{E}$ is the expectation operator. Define the estimate error as $\tilde{U} = U - \hat{U}$. The estimate error covariance is given by

$$P = \mathcal{E}\{\tilde{U}\tilde{U}^T\} = \Sigma^{-1}\,. \tag{16}$$

The diagonal entries of P are the error covariances for each point in the lattice Ω. The off-diagonal entries are the cross-covariances. Note that P is only a function of a priori information and can, therefore, be computed before any data is taken. The ability to compute an a priori error covariance gives our method an advantage over the methods proposed in [12, 11]. We plan to use this error covariance in future research to compute the minimum number and placement of tags to achieve a given reconstruction accuracy.

3.4 Transformation to material coordinates

The reconstructed displacement field given by Equation (13) is in spatial coordinates because the measurements are in spatial coordinates. The displacement field must be transformed to material coordinates before quatities such as strain can be computed. The main steps in our transformation method are shown for a 2D displacement field in Figure 9. After reconstruction, the displacement field is defined in spatial coordinates on a regular lattice as shown in

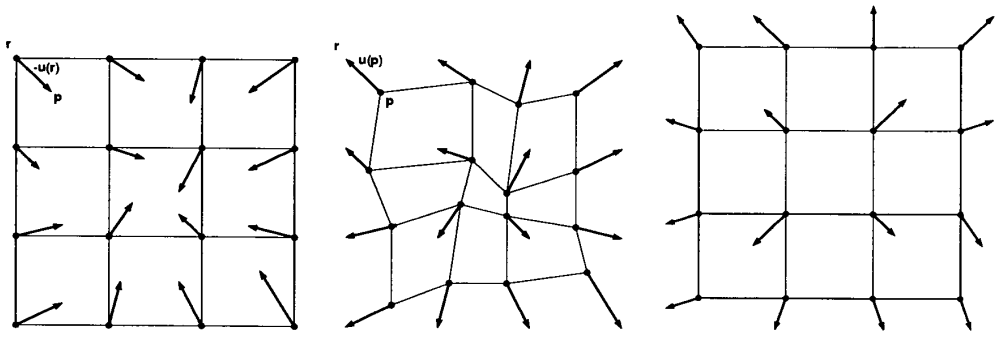

Figure 9: (a) Spatial coordinate displacement field defined on a regular lattice. (b) Material coordinate displacement field defined on an irregular lattice. (c) Material coordinate displacement field defined on a regular lattice.

Figure 9a. The spatial point $\mathbf{r}$ is related to the material point $\mathbf{p}$ by the equation

$$\mathbf{p} + \mathbf{u} = \mathbf{r}.$$

Since there is a one-to-one correspondence between the spatial points and the material points, we can also define $\mathbf{u}$ at the material points $\mathbf{p} = \mathbf{r} - \mathbf{u}$ as shown in Figure 9b. The displacement vectors are now defined on an irregular lattice, and an iterative technique is used to interpolate the material coordinate displacement field onto a regular grid as shown in Figure 9c.

4 Simulation results

To evaluate our 3-D displacement field interpolation method, we used a cardiac deformation simulator program written by Walter O'Dell. This program assumes the myocardium at end-diastole is a shell of a prolate sphere with inner radius 32mm and outer radius 40mm centered at the origin. It simulates a typical deformation taking place at end-systole [19]. It includes bulk translation, bulk rotation, and bulk shear, and torsion, transmural twist, transmural shear, and a gross compressibility constraint. Wireframe plots of the initial heart and the deformed heart are shown in Figures 10a and Figures 10b respectively. The reference map, which is needed to determine the positions of deformed tag planes from this deformation map, was determined by iterative approximation.

Simulated data from a 3-D planar tag imaging experiment was generated using the above model of left ventricular deformation. We assumed that in the short-axis images, 11 tags were separated by 5.5 mm and 11 images were separated by 5.0 mm. In the 11 long-axis images tags were separated by 5.0 mm and 11 long axis images were generated over 180 degrees. The position of deformed tag lines in each image were assumed to be known to pixel accuracy only. These numbers represent the type of data we expect to acquire in practice. Our 3-D displacement field reconstruction method was run on this data to estimate a complete displacement vector at each point on a $128 \times 128 \times 128$ lattice with a uniform spatial increment of 0.5625 mm. This result was compared to the known displacement, and a 3-D error map constructed. A volume-rendered version of this error map is shown in Figure 11a, where the grey level of each point is proportional to the absolute value of the error. Generally, the error is smallest near the apex and gets larger toward the base. This is revealed more clearly in a long-axis cross-section, shown in Figure 11b. A short-axis profile, shown in Figure 11c shows that errors are largest at the boundaries of the myocardium. This error is because outside the myocardium, the true displacement field is zero while inside the myocardium, the true displacement field is non-zero in general. The reconstruction algorithm smooths the estimate across the these discontinuities because the model described in Section 3.2. generates smooth displacement fields. We plan to address this problem in future research by confining the estimation domain to the myocardium itself instead of a cube. Table 1 shows the mean, root-mean-square (RMS), root-median-square (RMdS), av-

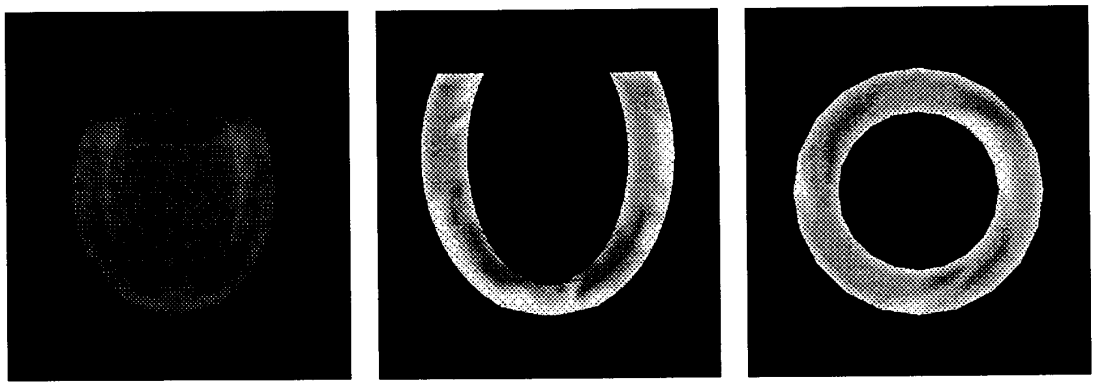

(a) (b) (c)

Figure 11: 3-D tag interpolation error: (a) volume-rendered 3-D version; (b) long-axis section; and (c) short-axis section.

	Error			
	x	y	z	Mag
Mean	0.0554	0.2697	0.3376	
RMS	0.4858	0.6361	0.7555	1.1006
MdS	0.3337	0.3963	0.2325	0.7789
Avg %	46.5486	49.7496	22.0793	13.9918
Md %	18.2713	13.0846	6.8682	12.8331

Table 1: Reconstruction errors (mm).

erage percent, and average median error for this reconstruction. These global errors are close to those obtained in basis function reconstruction method of O'Dell et al. [12] and the finite element method of Young and Axel [11].

The accuracy of our 3-D displacement field reconstruction method depends on the variances σ_w^2 and σ_s^2. While the measurement noise variance, σ_w^2, is derived from the tag tracker accuracy and the spatial increment, the σ_s^2 is usually chosen empirically. In the above simulation, we used $\sigma_w = 0.2813$ mm (one half of the spatial increment), and $\sigma_s^2 = 500$. To study the affect of σ_s^2 on the estimation accuracy, we computed reconstructions for several values of σ_s^2. The RMS error between the magnitudes of the reconstructed and actual displacement vectors versus σ_s^2 is plotted in Figure 12, where it is readily seen that the reconstruction error is fairly constant for the last 1.5 decades of σ_s^2. This result means that our reconstruction method is fairly robust to the choice of σ_s^2 provided that σ_s^2 is in the proper range.

5 Discussion

In this paper we presented a method for reconstructing the 3D displacement field of the heart on a regular 3D lattice from planar tagged images of the myocardium. This method uses a multidimensional stochastic model for the displacement field and the Fisher estimation framework to reconstruct a displacement vector at each point the lattice.

Simulation results show that the reconstruction accuracy is comparable to other methods proposed in [12, 11]. The reconstruction algorithm, however, smooths over discontinuities causing an increase in error at the boundaries of the myocardium. We plan to address this problem in future work by solving the reconstruction equation only at points inside the myocardium. Another area for potential improvement is the development of more sophisticated stochastic displacement field models that incorporate a divergence-free constraint, spatially varying process noise variances and deterministic heart models.

Other areas of future work include application of our reconstruction methods to actual MR cardiac images and use of the reconstruction error covariance in Equation (16) to determine the minimum number and placement of tags to achieve a given reconstruction accuracy.

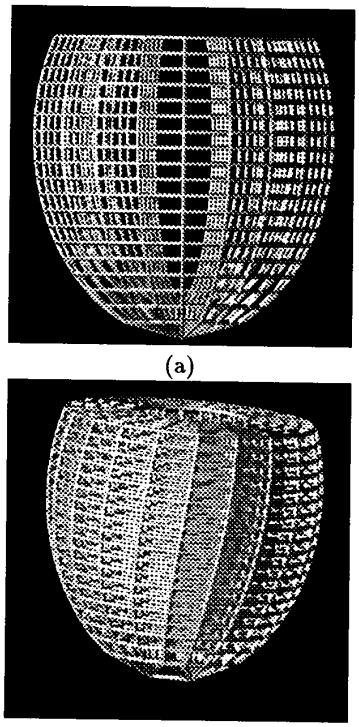

Figure 10: Wireframe rendering of simulated (prolate-spheroidal) left-ventricle: (a) initial configuration; (b) deformed configuration.

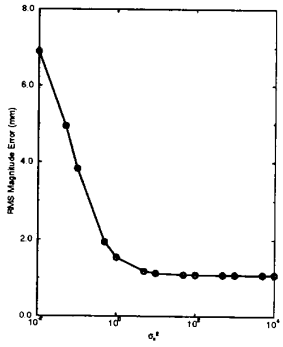

Figure 12: Displacement field reconstruction error vs. σ_s^2.

Acknowledgement:

We thank Walter O'Dell, M.S. for the use of his cardiac deformation simulator program and Elliot McVeigh, Ph.D. and Elias Zerhouni, M.D. for many insightful discussions on cardiac tagging.

References

[1] E.A. Zerhouni, D.M. Parish, W.J. Rogers, A. Yangand, and E .P. Shapiro. Human heart: tagging with MR imaging — a method for noninvasive assessment of myocardial motion. *Radiology*, 169:59–63, 1988.

[2] E.A. Zerhouni, E.R. McVeigh, J.L. Prince, B. Bolster, G. Hill, M. Guttman, S. Bouton, J. Lima, and J. Weiss. Dynamic 3d mapping of left ventricular contraction. In *SMRI Eighth Annual Meeting Program and Abstracts.* Pergamon Press, 1990.

[3] L. Axel and L. Dougherty. MR imaging of motion with spatial modulation of magnetization. *Radiology*, 171:841–845, 1989.

[4] L. Axel and L. Dougherty. Heart wall motion: improved method of spatial modulation of magnetizati on for MR imaging. *Radiology*, 172:349, 1989.

[5] M.A. Guttman and J.L. Prince. Image analysis methods for tagged MRI cardiac studies. In *Medical Imaging IV: Image Processing.* Bellingham WA: SPIE, 1990.

[6] B. D. Bolster, E. R. McVeigh, and E. A. Zerhouni. Myocardial tagging in polar coordinates with use of striped tags. *Radiology*, 177:769–72, 1990.

[7] E.R. McVeigh, B.D. Bolster, and E.A. Zerhouni. Striped TAGs (STAG) for measuring myocardial deformation. In *Magn. Reson. Imaging 8(suppl. 1)*, page 71. SMRI Eighth Annual Meeting, 1989.

[8] V.J. Wedeen, G. Homvang, H. Kantor, and T.J. Brady. Measurement of myocardial strain with phase sensitive MR. In *Proc. Soc. Mag. Res. in Medicine*, page 462. Soc. Mag. Res. Medicine, 1990. Annual Meeting, abstract only.

[9] M.A. Guttman, J.L. Prince, and E.R. McVeigh. Tag and contour detection in tagged MR images of the left ventricle, 1992. submitted to *IEEE Transactions on Medical Imaging.*

[10] D.B. Goldgof. Techniques for the left ventricle wall motion analysis. In *The Whitaker Foundation*

Snowbird Conference Abstracts, page unnumbered. The Whitaker Foundation, 1993.

[11] A. A. Young and L. Axel. Three-dimensional motion and deformation of the heart wall: estimation with spatial modulation of magnetization – a model-based approach. *Radiology*, 185:241–247, 1992.

[12] W. G. O'Dell, C. C. Moore, and E. R. McVeigh. Displacement field fitting approach to calculate 3d deformations from parallel-tagged MR images. *J. Magn. Reson. Imag.*, 3 (P):P208, 1993.

[13] M.A. Guttman, J.L. Prince, and E.R. McVeigh. Tag and contour detection in tagged MR images of the left ventricle. *IEEE Transactions on Medical Imaging*, 1993. accepted.

[14] F.C. Schweppe. *Uncertain Dynamic Systems.* Prentice-Hall, Inc., Englewood Cliffs, NJ, 1973.

[15] A. Rougee, B. C. Levy, and A. S. Willsky. Optic flow estimation inside a bounded domain. Technical Report Technical Report LIDS-P-1589, MIT Laboratory for Information and Decision Systems, 1986.

[16] A. Rougee, B. C. Levy, and A. S. Willsky. Reconstruction of two-dimensional velocity-fields as a linear-estimation problem. In *First International Conf. on Computer Vision*, pages 646–650, London, England, June 1987.

[17] T.M. Chin. *Dynamic estimation in computational vision.* PhD thesis, Massachusetts Institute of Technology, 1991.

[18] C.-C.J. Kuo, B.C. Levy, and B.R. Musicus. A local relaxation method for solving elliptic pdes on mesh-connected arrays. *SIAM J. Sci. Stat. Comput.*, 8(4):550–573, 1987.

[19] T. Arts, W.C. Hunter, A. Douglas, A.M.M. Muijtjens, and R.S. Reneman. Description of the deformation of the left ventricle by a kinematic model. *J. Biomechanics*, 25(10):1119–1127, 1992.